Determining the strength of magnetic and potential scattering of magnetic impurities on the surface of a topological insulator via quantum corrals

C. Zheng,[1] Q. L. Li,[1] B. F. Miao,[1,2] L. Sun,[1,2] R. Wang,[1] X. X. Li,[1] and H. F. Ding[1,2,*]

[1]*National Laboratory of Solid State Microstructures and Department of Physics, Nanjing University, 22 Hankou Road, Nanjing 210093, P. R. China*

[2]*Collaborative Innovation Center of Advanced Microstructures, Nanjing University, 22 Hankou Road, Nanjing 210093, P. R. China*

(Received 12 September 2017; published 29 December 2017)

We present the study of the effect of both magnetic and potential scattering (M and U) of magnetic impurities on the local electronic structures on a topological insulator. For single impurity, the local density of states (LDOS) shows distinct patterns of two resonance states with the positions depending on the relative strength of magnetic and potential scattering M and U. However, in the usual case where U is much larger than M, these two resonance states have very similar energy and become indistinguishable. Thus only one single peak is present, in analog with the experimental observations by scanning tunneling spectroscopy and providing a possible explanation for the recent debate among different experimental results. Interestingly, the effect of M can be significantly magnified when the magnetic impurities are forming nanosized quantum corrals, the apparent different features in the LDOSs allow justifying the existence of M despite its relative smaller strength compared with U. Remarkably, we find a one-to-one correspondence between the strength of U, M, and the energy positions of the quantum well states, giving a unique scheme to determine both U and M, which are of great importance for future TI based novel device design.

DOI: 10.1103/PhysRevB.96.235444

I. INTRODUCTION

Topological insulators (TIs) are a new state of quantum matter, which is insulating in bulk but hosts metallic surface states with a Dirac-like dispersion [1,2]. Due to the strong spin-orbit coupling, the spins of the surface states are perpendicularly locked to their momenta. These states are topologically protected in the sense that they are robust against small perturbations and cannot be destroyed by the presence of defects and adsorbates as long as the time-reversal symmetry (TRS) is preserved. These intriguing properties make TIs a very attractive material for spintronics [3,4] and topological quantum computation [5], etc.

Magnetic doping is of great interest in the study of TIs since it not only stimulates novel phenomena such as quantum anomalous Hall effect [6], but also holds the potential to open a band gap which is crucial for the TIs based devices [7–19]. Despite numerous experimental [7–15] and theoretical studies [16–19], the discussion on whether the magnetic impurities can induce the band gap, however, still remains controversial. Recent experiments showed that bulk doping of magnetic impurities can introduce a gap at the Dirac point [7,8]. In contrast, the effect of the surface doping is of strong debate. It was reported that the heavy doping of Fe can induce an energy gap [9], while other similar studies, however, found no gap [10–13]. More strikingly, several studies even reported that there is no apparent difference between the surface doping with magnetic and nonmagnetic impurities [14,15]. This raised the question whether the doped impurities are magnetic or not. The x-ray magnetic circular dichroism (XMCD), however, revealed the magnetism by the magnetic hysteresis loops [10,20–22]. To clarify this controversy, several mechanisms such as the spin-flipping inelastic scattering by the in-plane magnetic anisotropy of the magnetic impurities have been proposed [13,23–25]. Interestingly, Black-Schaffer *et al.* [25] calculated the band gap by taking into account both the magnetic and potential scattering M and U, and found the gap opening strongly depends on the relative strength of M and U. Under certain conditions, the gap opened by M can be refilled by the resonance states introduced by U [17].

The magnetic and potential scattering M and U are the two fundamental parameters used to describe the electron scattering of the magnetic impurities. They govern the influence of magnetic impurities on their hosts and thus control the properties of the newly generated state after doping. Despite their importance and the fact that they are commonly used in various theoretical approaches, their strengths seem to be only available via *ab initio* calculations [10,26,27]. If they can also be experimentally probed, it would be very helpful to understand the physical mechanism of the emerging phenomena and to design the materials for the exact needs of the novel applications. Therefore, it is highly desired to develop a method to measure the strength of both U and M. Moreover, the determination of these two important parameters may also provide an important check for the gap opening problem which is currently in hot debate.

In this paper, utilizing a T-matrix method, we systematically investigate the local electronic structures in the presence of magnetic impurities with both U and M on the surface of a TI. In particular, we study the single impurity case and find that the local density of states (LDOS) near a single impurity in general exhibits two resonance states in the presence of both U and M. And the LDOS can exhibit rich features depending on the relative strength of U and M. When U is much larger than M, which is the typical case, these two resonance states are located at an almost the same energy position and become indistinguishable. Thus only one single peak is present, in analog with the experimental observations by scanning tunneling spectroscopy (STS). This reconciles

*hfding@nju.edu.cn

the contradiction between the magnetic anisotropies of the magnetic impurities proved by the XMCD measurements and the nonmagnetic behavior in the STS [10,20–22]. We further propose a scheme to magnify the effect of M in the STS and determine the strength of U and M using quantum corrals. Quantum corrals can be built by atomic manipulation [27,28] and have been widely used to reveal the properties of complex electronic systems [29–32]. When the quantum corral is built by magnetic impurities, the backward scattering is no longer hindered due to the breaking of the TRS, thus resulting in a pronounced interference pattern inside the quantum corral. Due to the focusing effect at the center of the quantum corral, the effect of M can be significantly amplified. We calculate the LDOS and the spin-polarized LDOS (SP-LDOS) at the center of the corrals with different U and M. Remarkably, we find a one-to-one correspondence between the strength of U, M, and the energy positions of the quantum well states (QWS), giving a unique scheme to determine both U and M. The essential physics in quantum corrals can also be understood using an analytical model as discussed. The determination of both U and M may not only solve the remaining hot debate on the gap opening problem but also have great importance for future TI based device design.

The remaining part of the paper is organized as follows. In Sec. II we introduce a model to describe the impurities on a TI surface using T-matrix method. In Sec. III we show the results for the single impurity. Section IV is devoted to quantum corrals with different U and M. And the paper is summarized in Sec. V.

II. MODEL AND FORMALISM

We model the TI surface states by a low-energy effective massless Dirac Hamiltonian:

$$H_0 = \hbar v_f \boldsymbol{\sigma}\cdot\mathbf{k}, \tag{1}$$

where v_f is the Fermi velocity, $\boldsymbol{\sigma}=(\sigma_x,\sigma_y,\sigma_z)$ is the vector of Pauli matrices, and $\mathbf{k}=(k_x,k_y)$ is the planar momentum. With the band cutoff Λ, the short-range cutoff can be obtained as $a=\hbar v_f/\Lambda$. In our calculation we took $v_f = 4.6\times 10^5$ m/s and $\Lambda = 0.3$ eV, which are close to the typical values found in Bi_2Se_3, Bi_2Te_3, and Sb_2Te_3 [16,33–35]. The effect of impurities is described as $H_{\rm int}=\sum_i^N \mathbf{V}_i(\mathbf{r})$, $\mathbf{V}_i(\mathbf{r}) = (U\sigma_0 + J\mathbf{S}\cdot\boldsymbol{\sigma}/2)\delta(\mathbf{r}-\mathbf{r}_i)$, where $\mathbf{r}_i$ is the position of the ith pointlike impurity, U is the potential scattering strength, σ_0 is the 2×2 identity matrix, and J is the local Heisenberg exchange between the surface electrons and the impurity spin $\mathbf{S}$. Here we treat the impurity spin as a classical local magnetic moment with $M=JS/2$ under mean-field approximation. Note that if we integrate $H_{\rm int}$ over the two-dimensional space, the δ function will vanish, giving that U and M have the dimension [energy] $\times$ [length]^2 (see also Refs. [18,19]). Previously, most theoretical studies address the effect of the impurity on the LDOS with either pure potential or pure magnetic scattering [16–19,36,37]. In this paper we are going to discuss the case where both U and M exist and how the LDOS depends on their strengths.

To study the electronic structure in the presence of impurities on the surface of a TI, we employ a numerical T-matrix method [17,27,38,39] (we use the same notation as in Ref. [17]). The total LDOS (spin-unresolved) $\rho(\mathbf{r},\omega)$ and the SP-LDOS (spin up/down in direction μ) $\rho^{\mu}_{\pm}(\mathbf{r},\omega)$ can be calculated from the Green's function of the system $G(\mathbf{r},\mathbf{r}',\omega)$:

$$\rho(\mathbf{r},\omega) = -\frac{1}{\pi}\mathrm{Im}\{\mathrm{Tr}[G(\mathbf{r},\mathbf{r},\omega)]\}, \tag{2}$$

$$\rho^{\mu}_{\pm}(\mathbf{r},\omega) = -\frac{1}{\pi}\mathrm{Im}\left\{\mathrm{Tr}\left[G(\mathbf{r},\mathbf{r},\omega)\frac{1\pm\sigma_\mu}{2}\right]\right\}, \quad \mu = x,y,z. \tag{3}$$

According to the T-matrix method, the Green's function is determined by

$$G(\mathbf{r},\mathbf{r}',\omega) = G_0(\mathbf{r},\mathbf{r}',\omega) + \sum_{i,j=1}^{N} G_0(\mathbf{r},\mathbf{r}_i,\omega)T(\mathbf{r}_i,\mathbf{r}_j,\omega)G_0(\mathbf{r}_j,\mathbf{r}',\omega). \tag{4}$$

In it, $G_0(\mathbf{r},\mathbf{r}',\omega)$ is the free Green's function of TI surface without any impurity [17,38]:

$$G_0(\mathbf{r},\mathbf{r}',\omega) = \frac{|\omega|}{4\hbar^2 v_f^2}[f_0(\omega,\rho)\sigma_0 + f_1(\omega,\rho)(\boldsymbol{\sigma}\cdot\hat{\boldsymbol{\rho}})], \tag{5}$$

where $f_0(\omega,\rho) = \mathrm{sgn}(\omega)Y_0 - iJ_0\Theta(1-|\omega|/\Lambda)$, $f_1(\omega,\rho) = iY_1 + \mathrm{sgn}(\omega)J_1\Theta(1-|\omega|/\Lambda)$, J_i and Y_i are the Bessel function of the first and second kind, $|\omega|\rho/\hbar v_f$ is the argument of all the Bessel functions, and $\boldsymbol{\rho}=\mathbf{r}-\mathbf{r}'$. The on-site free Green's function can be derived as [17,40]

$$G_0(\mathbf{r},\mathbf{r},\omega) = -[g_0(\omega) + ig_1(\omega)]\sigma_0, \tag{6}$$

where

$$g_0(\omega) = \frac{\omega}{4\pi\hbar^2 v_f^2}\ln\left|\frac{\Lambda^2}{\omega^2}-1\right|,$$
$$g_1(\omega) = \frac{|\omega|}{4\hbar^2 v_f^2}\Theta\left(1-\frac{|\omega|}{\Lambda}\right). \tag{7}$$

The T-matrix contains the information about the propagation between the impurities, and it is determined by Dyson's equation:

$$T(\mathbf{r}_i,\mathbf{r}_j,\omega) = V_i\delta_{i,j} + V_i\sum_{l=1}^{N} G_0(\mathbf{r}_i,\mathbf{r}_l,\omega)T(\mathbf{r}_l,\mathbf{r}_j,\omega). \tag{8}$$

In matrix form, the T matrix is cast into

$$\mathbf{T} = \mathbf{V} + \mathbf{V}\mathbf{G_0}\mathbf{T}, \tag{9}$$

where

$$\mathbf{G_0} = \begin{pmatrix} G_0(\mathbf{r}_1,\mathbf{r}_1,\omega) & G_0(\mathbf{r}_1,\mathbf{r}_2,\omega) & \cdots & G_0(\mathbf{r}_1,\mathbf{r}_N,\omega) \\ G_0(\mathbf{r}_2,\mathbf{r}_1,\omega) & G_0(\mathbf{r}_2,\mathbf{r}_2,\omega) & \cdots & G_0(\mathbf{r}_2,\mathbf{r}_N,\omega) \\ \vdots & \vdots & \ddots & \vdots \\ G_0(\mathbf{r}_N,\mathbf{r}_1,\omega) & G_0(\mathbf{r}_N,\mathbf{r}_2,\omega) & \cdots & G_0(\mathbf{r}_N,\mathbf{r}_N,\omega) \end{pmatrix}, \tag{10}$$

$$\mathbf{V} = \begin{pmatrix} \mathbf{V}_1 & 0 & \cdots & 0 \\ 0 & \mathbf{V}_2 & \cdots & 0 \\ \vdots & \vdots & \ddots & \vdots \\ 0 & 0 & \cdots & \mathbf{V}_N \end{pmatrix}, \tag{11}$$

since each $G_0(\mathbf{r}_i,\mathbf{r}_j,\omega)$ and $\mathbf{V}_i$ is a 2×2 matrix, $\mathbf{G_0}$, $\mathbf{V}$, and $\mathbf{T}$ are all $2N\times2N$ matrices. And the T matrix can be obtained by

$$\mathbf{T} = \mathbf{V}(\mathbf{I} - \mathbf{V}\mathbf{G_0})^{-1}, \tag{12}$$

where $\mathbf{I}$ is an $2N\times2N$ identity matrix. By solving Eq. (12) we can obtain the T matrix of this system. Again, by substituting the T matrix into Eq. (4), we can further derive the Green's function $G(\mathbf{r},\mathbf{r}',\omega)$ and consequently the LDOS and the SP-LDOS.

III. SINGLE IMPURITY

First, we consider the case of a single magnetic impurity on top of a TI surface. The problem of a single impurity with pure U or M was previously studied by Biswas *et al.* [17]. They found that a nonmagnetic impurity introduces a single resonance state near the Dirac point, the spectrum is doubly degenerate due to the Kramers' theorem. A magnetic impurity breaks the TRS. The spectrum thus becomes nondegenerate and two symmetric spin-polarized resonance states appear at each side of the Dirac point. As the strength of the potential increases, the peaks become narrower and move towards the Dirac point.

In the following, we consider the case when both U and M exist. In such condition, the additional term $GTG \equiv \delta G$ in the Green's function (4) can be derived as (using $g = g_0 + ig_1$)

$$\begin{aligned}\delta G = {} & \frac{\omega^2}{16\hbar^4 v_f^4[1+(U-M)g][1+(U+M)g]} \\ & \times\big\{-2i f_0 f_1 M\boldsymbol{\sigma}\cdot(\mathbf{S}\times\hat{\mathbf{r}}) + \big(f_0^2+f_1^2\big)M\boldsymbol{\sigma}\cdot\mathbf{S} \\ & - 2f_1^2 M(\boldsymbol{\sigma}\cdot\hat{\mathbf{r}})(\mathbf{S}\cdot\hat{\mathbf{r}}) + [U+(U^2-M^2)g]\big(f_0^2-f_1^2\big)\big\}.\end{aligned} \tag{13}$$

By setting $M = 0$ or $U = 0$, one can easily find that this formula can be simplified to the pure U or the pure M case as given in Ref. [17]. With Eq. (13), one can deduce the positions of the peaks caused by the resonance states and calculate both the LDOS and the SP-LDOS numerically. For simplicity, we limit our discussion to a z-polarized magnetic impurity, the results of x-polarized and y-polarized impurities can be obtained in a similar manner. In order to illustrate how the spectrum transforms from the case with pure magnetic scattering to the potential scattering dominated case, we fix M and vary U to explore the evolution of the spectrum near a single impurity. For comparison, we first adopt the same parameters in Ref. [17], namely $M = 100\Lambda a^2 = 30$ eV nm^2, $r = 20$ nm. We note that we only use these parameters for the comparison here. For the rest of the paper, we use more realistic parameters.

Figure 1 illustrates the evolution of both the LDOS and SP-LDOS near a magnetic impurity with increasing the ratio of U/M. Depending on the relative strength of U and M, the spectrum shows different patterns of resonance states. The physical origin of the evolution can be understood as follows. As the imaginary part of the Green's function gives the LDOS, the peak positions correspond to the energy where the denominator $[1+(U-M)g][1+(U+M)g]$ is

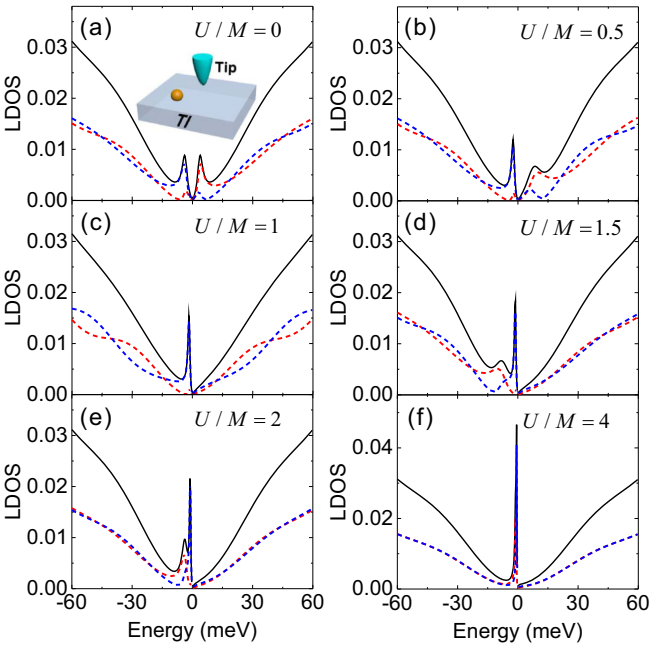

FIG. 1. Evolution of LDOS (solid black lines) and SP-LDOS (spin-up: dotted red line, spin-down: dotted blue line) near a single magnetic impurity for different ratio of U/M. The inset shows a sketch of the experimental setup. Here $M = 30$ eV nm^2, $r = 20$ nm.

minimized. Since $U+M$ is always positive, the minimum of $1+(U+M)g$ corresponds to a resonance peak in the negative branch. In the limit of very large scattering strengths, $U+M \gg \Lambda a^2$, the energy position can be approximately obtained as $\Omega_1 \approx -2\pi\hbar^2 v_f^2/(U+M)\ln\frac{\Lambda(U+M)}{2\pi\hbar^2 v_f^2}$. The peak position from the minimization of $1+(U-M)g$ depends on the relative strength of U and M. If $U < M$, it locates at $\Omega_2 \approx 2\pi\hbar^2 v_f^2/|U-M|\ln\frac{\Lambda|U-M|}{2\pi\hbar^2 v_f^2}$. That is, the peak will appear in the positive energy, as shown in Figs. 1(a) and 1(b). Increasing U will make both peaks move towards the positive direction. When $U = M$, the second peak disappears, there is only one peak in the negative range as shown in Fig. 1(c). Note that although only one spin component is scattered in this case, both two spin components can be affected due to the spin-momentum locking nature of the TI surface state. This can also be understood from Eq. (5), as the off-diagonal components in the free Green's function contain the $\boldsymbol{\sigma}\cdot\hat{\boldsymbol{\rho}}$ term, both spin components are renormalized by the impurity. In the case of $U > M$, the second peak will then appear in the negative range: $\Omega_2 \approx -2\pi\hbar^2 v_f^2/(U-M)\ln\frac{\Lambda(U-M)}{2\pi\hbar^2 v_f^2}$, as shown in Figs. 1(d)–1(f). As we continue to increase U, these two peaks will move to the positive direction and approach the Dirac point. In the case of $U/M \geqslant 4$ [see Fig. 1(f)], these two peaks are so close to each other and become almost indistinguishable, the spectrum is then highly degenerate similar to the impurity with the pure U case. To summarize, when both U and M exist, we will in general have two resonance peaks in the spectrum. From the positions of these two peaks, we can infer the relative strength of U and M, or even deduce the value of $U+M$ and $U-M$ so that we can obtain the value of U and M in a single STS spectrum.

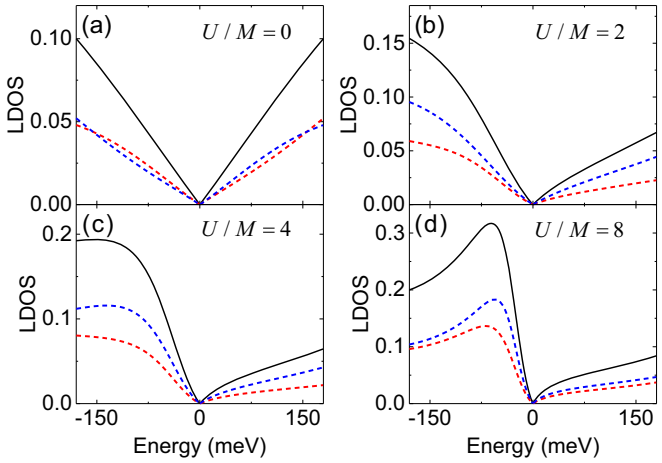

FIG. 2. Evolution of LDOS (solid black lines) and SP-LDOS (spin-up: dotted red line, spin-down: dotted blue line) near a single magnetic impurity for different ratio of U/M. Here $M = 0.45\,\mathrm{eV\,nm^2}$, $r = 1$ nm. [We note that (d) is similar to the spectra reported experimentally, see, e.g., Fig. 1 in Ref. [10], Fig. 1 in Ref. [20], and Fig. 2 in Ref. [21], etc.

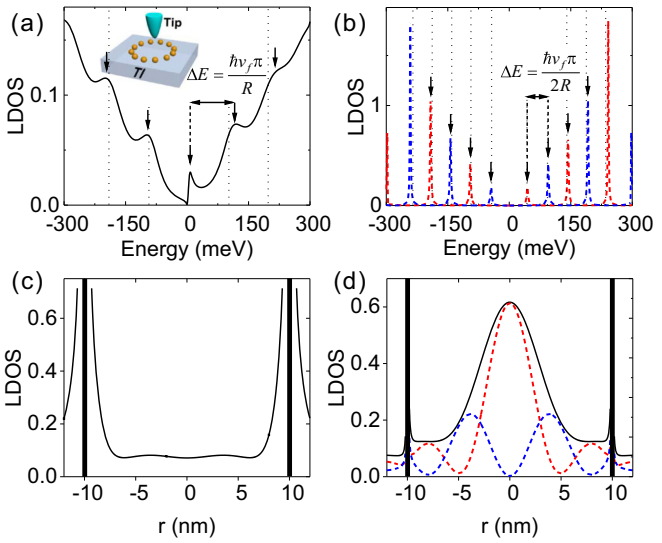

FIG. 3. LDOS (solid black lines) and SP-LDOS (spin-up: dotted red line, spin-down: dotted blue line) at the center of a circular quantum corral with (a) pure potential and (b) pure magnetic scattering. Inset: sketch of the experimental setup. The black arrows indicate the QWS of the corral. Here $U = 1.5\,\mathrm{eV\,nm^2}$, $M = 0.45\,\mathrm{eV\,nm^2}$, $R = 10$ nm, $N = 50$. The vertical thin dotted lines correspond to eigenenergies obtained via an analytical method with $U' = 1.5$ eV nm, $M' = 0.45$ eV nm. (c) and (d) The LDOS and SP-LDOS as a function of the position across the center of the corral with $E = 0.144$ eV, the thick vertical lines indicate the locations of the adatoms.

Recent STM experiments studied various magnetic impurities on different TIs, such as Fe, Co, and Mn on Bi_2Se_3 and Bi_2Te_3 [10,13,20–22], where the adatoms occupy either fcc or hcp sites with respect to the underlying TI surface lattice. Even though the XMCD measurements proved that they are magnetic in nature, the obtained STS does not show the typical two resonance peaks, but rather a single resonance peak similar to nonmagnetic impurities on TIs, in sharp contrast to the above discussion. In fact, we found that this discrepancy is originated from the fact that the parameters in the above discussion are far from the real material parameters. The parameters we used above are $M = 30\,\mathrm{eV\,nm^2}$, $r = 20$ nm, while the value of M/a^2 is typically in the range of 0.1–1 eV, and U/a^2 is about 1–10 eV [16,18,25]. Therefore, we take more realistic values, namely, $M = 0.45\,\mathrm{eV\,nm^2}$, $r = 1$ nm, and performed the calculation again. The results are shown in Fig. 2. When M is small, the two resonance peaks lie far away from the Dirac point and are not visible in the spectrum, as shown in Fig. 2(a). As U increases, the peaks move towards the positive direction. When $U/M = 8$, we obtain a similar spectrum as described in the experiments [10,13,20–22]. This suggests that a magnetic impurity has not only magnetic scattering but also strong potential scattering as described by Black-Schaffer *et al.* [25]. When M is small in comparison with U, it has only a small modification on the spectrum. In such a case, the main feature of the spectrum is dominated by U and only one peak is present. This explains the discrepancy between the results of the STS and XMCD measurements. The presence of only one peak, however, makes it difficult to extract the values of U and M simultaneously due to the rather limited information. In order to provide more evidence on the proposed mechanism and determine the values of U and M, we continue to discuss the quantum corral case in the following sections.

IV. QUANTUM CORRALS

As discussed above, the magnetic scattering strength from a single impurity is small and has little influence on the LDOS, making it difficult to reveal the magnetic properties of the impurities in the STS. In order to reveal this influence, we need to magnify the effect of M. This brings us to the idea of quantum corrals. Quantum corrals are two-dimensional structures that can be built by atomic manipulation [27,28]. Due to the breaking of the TRS, the backscattering of the surface electrons by the magnetic impurities is no longer hindered, causing the standing wave inside the quantum corral. Due to the focusing effect at the center of the corral, the effect of M can be magnified more in comparison with the effect of U and may result in the distinguishable feature in STS at the corral center.

A. Quantum corrals with pure U or M

Before discussing the general situation where both U and M exist, we briefly summarize the case of quantum corrals with either pure U or M, which was performed by Fu *et al.* [39]. In the pure M case, according to previous studies [16–19], the mediated helical Dirac electrons lead to ferromagnetic Ruderman-Kittel-Kasuya-Yosida (RKKY) interaction among the magnetic adatoms on the surface of TIs, thus a ferromagnetic easy axis along the z axis is preferred. In Fig. 3 we present the spectra at the center of a circular corral with the radius of 10 nm and comprising of 50 adatoms on the surface of a TI for the case of pure $U(=1.5\,\mathrm{eV\,nm^2})$

and pure $M(=0.45\,\mathrm{eV\,nm^2})$, respectively. The differences between these two are dramatic. They not only have different symmetries but also have different energy spacing between the neighboring energy levels. In the pure U case, the TRS is preserved, so the spin-up and spin-down components are degenerate based on the Kramers' theorem. While in the pure M case, the TRS is broken, thus the spin-up and spin-down components become nondegenerate. Although TRS is broken in this case, there is an additional symmetry when the magnetic moments of the impurities are along the z axis, namely the particle-hole symmetry. As it can be noticed that if ψ is an eigenstate of H with energy E, under the transformation $\psi' = \sigma_x \psi^*$ the H will transform to $-H$. Thus the spectrum will be symmetric with respect to $E = 0$ [41].

The basic role of the quantum corral is to confine the surface state electrons and introduce discrete QWS in the spectrum. Since the potential scattering cannot backscatter the massless Dirac fermions, the quantum confinement effect of the surface state electrons of TI in the pure U case is strongly suppressed [see also Fig. 3(c), the line profile of the LDOS across the corral center]. Thus, the widths of the QWS are broad in this case, expressing short lifetimes of the quasibound states. On the other hand, the surface state electrons can be backscattered by the magnetic impurities due to the breaking of the TRS. Thus, they can be confined in the pure M case and pronounced quantum confinement effect is present [see also Fig. 3(d), the line profile of the LDOS/SP-LDOS across the corral center]. The QWS become very sharp, expressing very long lifetimes of the resonant states. If M is sufficiently large, there will be an energy gap near the Dirac point, while in the pure U case there is a typical resonance peak located at the Dirac point. Similar to quantum corrals on an ordinary metallic surface, the energy positions of QWS are determined by the size of the corral [28]. Due to the different dispersion relationships (linear for the surface state on top of TI and parabolic for the surface state on an ordinary metal), the explicit energy positions of the QWS are different for quantum corrals on top of a TI or an ordinary metal which possess a surface state. This can also be understood by an analytical model which will be presented below.

B. Analytical model of quantum corrals on TI surface

In order to gain a better understanding of the physics of the numerical results by the T-matrix method, we develop an analytical model of quantum corrals on a TI surface. In it, we model the circular corral as a continuous barrier with the form

$$V(r) = (U'\sigma_0 + M'\sigma_z)\delta(r - R), \tag{14}$$

where r is the distance to the center of the circle and R is the radius. Note that U' and M' introduced here are not the same as the U and M we introduced in the previous sections, they have different dimensions. If we integrate $V(r)$ over the radial direction, the δ function will vanish, giving that U' and M' have the dimension [energy] $\times$ [length] (see also Ref. [42]). We solve the Dirac equation $H_0\psi + V(r)\psi = E\psi$ to obtain the eigenenergies, where H_0 refers to the unperturbed massless Dirac Hamiltonian in Eq. (1). Due to the rotational symmetry, it is natural to write the equation in polar coordinates (r,θ), namely

$$-i\hbar v_f \begin{pmatrix} 0 & e^{-i\theta}\left(\frac{\partial}{\partial r} - i\frac{1}{r}\frac{\partial}{\partial\theta}\right) \\ e^{i\theta}\left(\frac{\partial}{\partial r} + i\frac{1}{r}\frac{\partial}{\partial\theta}\right) & 0 \end{pmatrix}\begin{pmatrix}\psi_1\\ \psi_2\end{pmatrix} + V\begin{pmatrix}\psi_1\\ \psi_2\end{pmatrix} = E\begin{pmatrix}\psi_1\\ \psi_2\end{pmatrix}. \tag{15}$$

For the cylindrically symmetric potential, the two-component wave function has the following form:

$$\psi_l = e^{il\theta}\begin{pmatrix} u(r) \\ ie^{i\theta}v(r)\end{pmatrix}. \tag{16}$$

Inside and outside of the corral, $V = 0$, it has the regular solution [41]

$$\begin{aligned} \psi_l &= e^{il\theta}\begin{pmatrix} J_l(\varepsilon r/R) \\ ie^{i\theta}J_{l+1}(\varepsilon r/R)\end{pmatrix}, && \text{if } r < R, \\ \psi_l &= e^{il\theta}A_l\begin{pmatrix} {H^{(1)}}_l(\varepsilon r/R) \\ ie^{i\theta}{H^{(1)}}_{l+1}(\varepsilon r/R)\end{pmatrix} \\ &\quad + e^{il\theta}B_l\begin{pmatrix} {H^{(2)}}_l(\varepsilon r/R) \\ ie^{i\theta}{H^{(2)}}_{l+1}(\varepsilon r/R)\end{pmatrix}, && \text{if } r > R, \end{aligned} \tag{17}$$

where l is the orbital angular momentum, J_l is the Bessel function of the first kind, ${H^{(1)}}_l$ (${H^{(2)}}_l$) is the Hankel function of the first (second) kind, and we also introduced the dimensionless energy $\varepsilon = RE/\hbar v_f$. The solutions are eigenfunctions of the z component of the total angular momentum:

$$\hat{L}\psi_l = \left(-i\partial_\theta + \tfrac{1}{2}\sigma_z\right)\psi_l = \left(l + \tfrac{1}{2}\right)\psi_l. \tag{18}$$

As we are mainly interested in the spectrum at the center of the corral, we treat $l = 0, -1$.

In order to figure out the eigenenergies of the system, we impose the so-called outgoing boundary condition [43,44], that is, $B_l = 0$. The most important information of the system locates at the boundary of the corral, where U' and M' play their roles and make all the differences. Here we are dealing with the Dirac equation (first order in the space derivative) with δ-like potential, the wave function itself will be discontinuous at $r = R$. Substituting Eq. (16) into Eq. (15) we can obtain an equation for the spinor $\phi(r) = \binom{u(r)}{v(r)}$:

$$\frac{d\phi(r)}{dr} = \hat{K}(r)\phi(r), \tag{19}$$

where

$$\hat{K} = \begin{pmatrix} \frac{l}{r} & -\frac{\varepsilon}{R} + (\mathcal{U}' - \mathcal{M}')\delta(r - R) \\ \frac{\varepsilon}{R} - (\mathcal{U}' + \mathcal{M}')\delta(r - R) & -\frac{l+1}{r}\end{pmatrix}. \tag{20}$$

In it, we introduced the dimensionless potential $\mathcal{U}' = U'/\hbar v_f$ and $\mathcal{M}' = M'/\hbar v_f$. Integrating both sides of the equation near $r = R$, we find the following boundary condition:

$$\begin{pmatrix} u(R^+) \\ v(R^+)\end{pmatrix} = \mathbf{M}_{mn}\begin{pmatrix} u(R^-) \\ v(R^-)\end{pmatrix}, \tag{21}$$

where $\mathbf{M}_{mn}$ is the transfer matrix:

$$\mathbf{M}_{mn} = \frac{1}{4+\mathcal{U}'^2-\mathcal{M}'^2} \times \begin{pmatrix} 4-(\mathcal{U}'^2-\mathcal{M}'^2) & 4(\mathcal{U}'-\mathcal{M}') \\ -4(\mathcal{U}'+\mathcal{M}') & 4-(\mathcal{U}'^2-\mathcal{M}'^2) \end{pmatrix}. \quad (22)$$

In the derivation we use the property of the δ function that $\lim_{\eta\to 0}\int_{-\eta}^{\eta} f(x)\delta(x)dx = \frac{1}{2}[f(-\eta)+f(+\eta)]$. From this condition we can find the energy eigenvalue equation, which takes the form

$$\frac{H^{(1)}{}_l(\varepsilon)}{H^{(1)}{}_{l+1}(\varepsilon)} = \frac{\mathbf{M}_{11}J_l(\varepsilon)+\mathbf{M}_{12}J_{l+1}(\varepsilon)}{\mathbf{M}_{21}J_l(\varepsilon)+\mathbf{M}_{22}J_{l+1}(\varepsilon)}. \quad (23)$$

The solution of the eigenvalue equation determines the complex energy spectrum of the corral, the real part of the complex energy gives the energy position of the QWS; the imaginary part gives the inverse of the lifetime. Note that the above equation may also be useful in the analysis of the quantum dot problem on TIs [45,46] and graphene [47–49]. From Eq. (23) we can clearly see that the eigenenergies are determined by the radius R and U', M' imposed on the boundary. For a given angular momentum l, we can solve it numerically. For $U' = 1.5$ eV nm, $M' = 0$ and $U' = 0$, $M' = 0.45$ eV nm, the results are shown in Fig. 3 as the vertical thin dotted lines, they are in good agreement with the results obtained with the T-matrix method. It turns out that the analytical solutions to Eq. (23) can be obtained in the limit of $\varepsilon \gg 1$. In the pure M case, Eq. (23) becomes

$$J_l(\varepsilon)H^{(1)}{}_l(\varepsilon) - J_{l+1}(\varepsilon)H^{(1)}{}_{l+1}(\varepsilon) = -\frac{1}{i\pi\varepsilon}\frac{4+\mathcal{M}'^2}{2\mathcal{M}'}. \quad (24)$$

By using the asymptotic forms of the Bessel functions:

$$J_l(\varepsilon) = \sqrt{\frac{1}{2\pi\varepsilon}}\left[e^{i(\varepsilon-\frac{l\pi}{2}-\frac{\pi}{4})}+e^{-i(\varepsilon-\frac{l\pi}{2}-\frac{\pi}{4})}\right],$$
$$H^{(1)}{}_l(\varepsilon) = \sqrt{\frac{2}{\pi\varepsilon}}e^{i(\varepsilon-\frac{l\pi}{2}-\frac{\pi}{4})}, \quad (25)$$

we obtain

$$e^{i(\varepsilon-l\pi-\frac{\pi}{2})(2)} - e^{i[2\varepsilon-(l+1)\pi-\frac{\pi}{2}]} = i\frac{4+\mathcal{M}'^2}{2\mathcal{M}'}. \quad (26)$$

Substituting $\varepsilon = \varepsilon_a - i\varepsilon_b$ into Eq. (26) allows us to write a couple of real equations:

$$\left\{\cos\left(2\varepsilon_a - l\pi - \frac{\pi}{2}\right) - \cos\left[2\varepsilon_a - (l+1)\pi - \frac{\pi}{2}\right]\right\}e^{2\varepsilon_b} = 0,$$
$$\left\{\sin\left(2\varepsilon_a - l\pi - \frac{\pi}{2}\right) - \sin\left[2\varepsilon_a - (l+1)\pi - \frac{\pi}{2}\right]\right\}e^{2\varepsilon_b} = \frac{4+\mathcal{M}'^2}{2\mathcal{M}'}. \quad (27)$$

The first equation gives us the energy position of the QWS:

$$\varepsilon_a = \frac{n\pi}{2}, \quad (28)$$

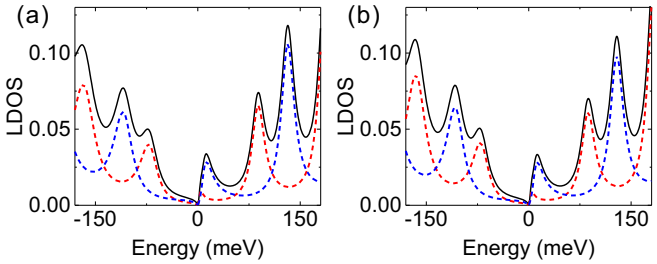

FIG. 4. LDOS (solid black lines) and SP-LDOS (spin-up: dotted red line, spin-down: dotted blue line) at the center of two different corrals whose effective M' and U' (NM and NU) are equal, their LDOSs also show almost the same pattern. Here $N = 50$, $M = 0.9\,\text{eV nm}^2$, $U = 1.8\,\text{eV nm}^2$, $R = 10$ nm in (a); $N = 100$, $M = 0.45\,\text{eV nm}^2$, $U = 0.9\,\text{eV nm}^2$, $R = 10$ nm in (b).

and the second equation gives us its decay width:

$$\varepsilon_b = \frac{1}{2}\ln\left(\frac{4+\mathcal{M}'^2}{4\mathcal{M}'}\right). \quad (29)$$

The decay width has a minimum at $\mathcal{M}' = 2$, which is consistent with the results of the T-matrix method.

In the pure U case, Eq. (23) becomes

$$J_l(\varepsilon)H^{(1)}{}_l(\varepsilon) + J_{l+1}(\varepsilon)H^{(1)}{}_{l+1}(\varepsilon) = -\frac{1}{i\pi\varepsilon}\frac{4-\mathcal{U}'^2}{2\mathcal{U}'}. \quad (30)$$

This equation cannot be solved by Eq. (25), which only includes the leading term of the Bessel functions. However, both the numerical results of Eq. (30) and the T-matrix method can be approximately described by $\varepsilon_a = n\pi$. In brief, the spacing between each eigenenergy is $\sim\hbar v_f\pi/R$ for the pure U case and $\sim\hbar v_f\pi/2R$ for the pure M case, respectively (see Fig. 3). We therefore can control the positions of the eigenenergies by changing the radius of the corral. Due to the different definitions between U, M and U', M', the results obtained by the analytical model and the numerical T-matrix method are not exactly the same. Furthermore, in the realistic circumstance, the corral is made of discrete adatoms instead of a continuous barrier. Increasing the number of the adatoms of the corral is equivalent to increasing the effective M' and U' of the boundary, so the spectrum in the corral is a function of NM and NU. As an example, Fig. 4 demonstrates the LDOSs and SP-LDOSs at the center of two different corrals whose effective M' and U' are equal, the spectra also show almost the same pattern.

In the case that both U' and M' exist, it is difficult to obtain the exact analytical solution for the eigenenergies. But we can still solve Eq. (23) numerically to obtain the energy positions of the QWS. As discussed above, the quantum corrals exhibit dramatically different properties for corrals formed by impurities with the pure U and pure M scattering. This suggests that the spectrum could be strongly dependent with both U and M in the general case, suggesting the possibility to determine the strength of both.

C. Quantum corrals with both U and M

In the following we proceed with the discussion for the case when both U and M exist. Similar to the single impurity case,

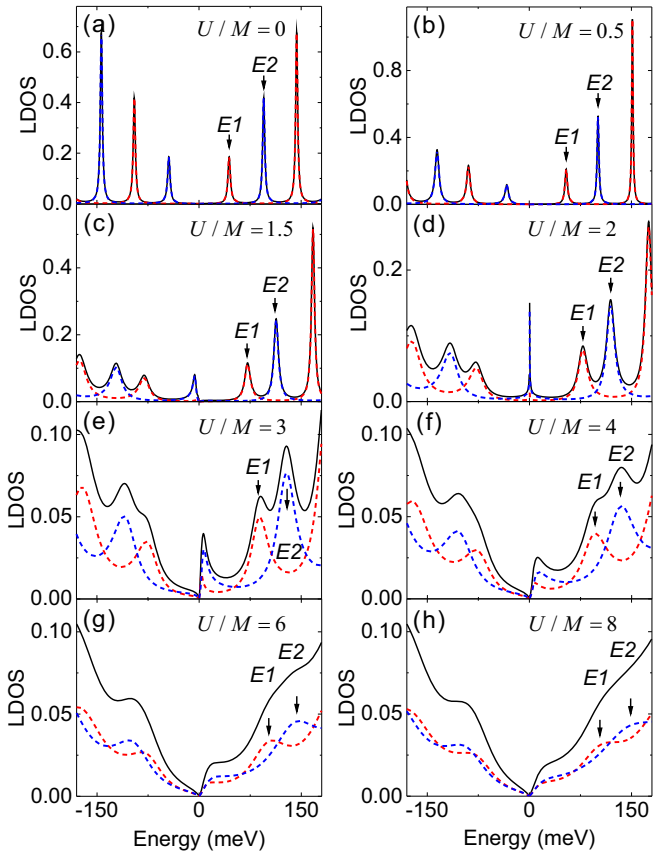

FIG. 5. Evolution of LDOS (solid black lines) and SP-LDOS (spin-up: dotted red line, spin-down: dotted blue line) at the center of the quantum corrals for different ratio of U/M. $E1$, $E2$ are the first two eigenmodes in the positive range. Here $M = 0.45\,\mathrm{eV\,nm^2}$, $R = 10$ nm, $N = 50$.

we fix M and vary U to explore the evolution of the spectrum at the center of the quantum corral. Figure 5 illustrates the results of different ratios U/M given by the T-matrix method when $M = 0.45\,\mathrm{eV\,nm^2}$. As mentioned above, the quantum corrals with pure U preserve the TRS while the pure M ones preserve the particle-hole symmetry. When both U and M exist, both symmetries will be broken. Thus the spectrum is neither degenerate nor symmetric with respect to $E = 0$, but has a mixed character depending on the relative strength of U and M. Similar to the single impurity case, the existence of U has two major effects on the spectrum: it makes the spectrum more degenerate and shifts the QWS. When U/M is small [see Figs. 5(a)–5(c)], the spectrum becomes asymmetric and moves towards the positive direction with increasing U/M due to the hole doping effect of U [25]. The ratio $U/M = 2$ is a critical one during the process [see Fig. 5(d)] (we note that this critical ratio is M dependent which will be further discussed in the next section). At this condition, the asymmetry becomes so drastic that the first negative eigenmode moves to the center of the spectrum. Due to the relative weakening of the magnetic scattering, the gap near the Dirac point also gradually closes. When $U/M < 3$, the process is dominated by the shift of the peak positions in the spectrum. If we increase the ratio further, the changes of the spectrum are dominated by the decreasing of the peak intensity and broadening of the peak width [see Figs. 5(f)–5(h)]. The spectrum becomes more and more degenerate as the difference between the spin-up and spin-down LDOS (the spin polarization) becomes smaller and smaller. In the case of $U/M = 8$, the spin-up and spin-down components are almost degenerate, similar to the pure U case.

D. Determination of the strength of U and M by the spectrum

Above, we show that the LDOS at the center of the quantum corral strongly depends on the strength of both U and M for a fixed M. In the following we will continue the discussion for the change of the spectrum with the variation of M. As shown in Fig. 5, the spectra show distinct features on the positions of the QWS and the spin polarization of the spectrum. In this paper we focus our discussion on the positions of the QWS since they are easier to be identified experimentally. For a corral with specific geometry (fixed diameter and number of impurities), the positions of the QWS only depend on U and M. Namely, they are the only functions of U and M. If we have the explicit form of these functions, we may be able to obtain U and M from the positions of the QWS. Since we have two unknown variables U and M, we need at least two equations to derive their values. Here we choose the first two eigenmodes in the positive range (as indicated by $E1$ and $E2$ in Fig. 5), other choices of eigenmodes are also feasible.

In Fig. 6 we plot $E1$ and $E2$ as the function of U/M for different M given by the T-matrix method. We note that similar results (not shown for avoiding redundancy) can also be obtained by numerically solving Eq. (23) in the analytical model. The symbols are the calculated values while the lines are the fittings that will be discussed below. Note that the choices of U and M cover almost all the realistic values [16,18,25]. We find that all the curves behave similarly, they all increase with increasing U/M. And the slopes of the curves decrease with increasing U/M. In addition, for a given U/M,

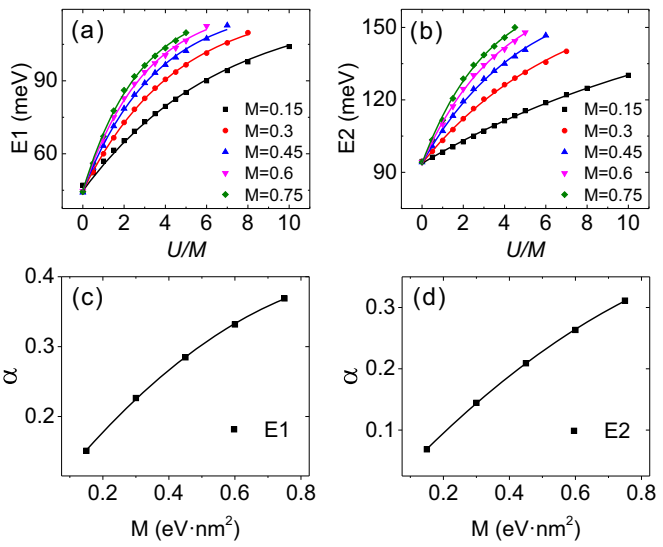

FIG. 6. (a) and (b) Calculated $E1$ and $E2$ as a function of U/M for different M, whose unit is $\mathrm{eV\,nm^2}$. (c) and (d) The fitted parameter α as a function of M for $E1$ and $E2$ (see text). Here $R = 10$ nm, $N = 50$.

the slope is higher if M is larger. Importantly, each value of $E1$ or $E2$ corresponds to a single set of U and M except that the curves merge at $U/M = 0$. Namely, when U and M are different, $E1$ or $E2$ are also different. This suggests that the determination of $E1$ and $E2$ may enable the estimation of U and M. The merging of the curves at $U/M = 0$ can be understood since the above discussed analytical model yields that the eigenenergy only depends on the radius of the corral when $U = 0$. The increasing of $E1$ and $E2$ with U/M can also be understood as the hole doping effect of U. When U/M is very large, the spectrum will behave like the pure U case and become degenerate. And $E1$ and $E2$ will eventually merge to a single value. Since $E1$ has to move a longer distance to coincide with $E2$, $E1$ will move at a faster speed than $E2$. This difference provides us the unique opportunity to derive the two unknown variables U and M simultaneously. Remarkably, we find that almost all the curves can be fitted by an exponential growth asymptotic function:

$$E = E_0 - Ae^{-\alpha U/M}. \tag{31}$$

And the fittings (lines) essentially reproduce the calculated results (symbols) very well (see Fig. 6). The physical meanings of these parameters can be understood as follows: $E_0 - A$ corresponds to the energy when $U/M = 0$, and it approximately equals $\hbar v_f \pi/2R$ for $E1$ and $\hbar v_f \pi/R$ for $E2$, respectively. This also explains why all the curves merge to a single value at $U/M = 0$. With increasing U/M, the eigenenergy will exponentially approach E_0. While the parameter α captures the different increasing speed of the eigenenergies for different M. The fittings yields $E_0 = 121.59$ meV and $A = 76.89$ meV for $E1$. While α exhibits some dependence on M as is shown in Fig. 6(c). The dependence is almost linear and can be described more accurately with $\alpha = 0.066 + 0.612M - 0.279M^2$. The fitting of $E2$ gives $E_0 = 167.37$ meV, $A = 73.68$ meV, and $\alpha = -0.015 + 0.592M - 0.210M^2$. Thus we obtain two explicit formulas for $E1$ and $E2$. When both of them are measured experimentally, we can deduce the value of U and M from these two formulas accordingly.

We can also examine our results by building corrals with different geometries. With U and M in hand, we can calculate the spectra in corrals with different sizes and compare the results with the experiments. As discussed above, for a corral with radius R, the spacing between each eigenenergy scales with $1/R$. Namely, a smaller R results in a larger spacing. The parameter E_0 and A in Eq. (31) will also scale with $1/R$. We confirm this by further studying quantum corrals with different radii. The obtained LDOS shows similar features and $E1$, $E2$ can still be well described by Eq. (31). The corresponding E_0 and A for different radii are shown in Fig. 7. They are almost proportional to $1/R$. In addition, the number of the adatoms of the corral will affect the effective M' of the corral as mentioned in the analytical model, if M is very small, we can increase the number to magnify the effect of M. To be more specific, when the number of the adatoms changes to N' (N' should not be too small to form a corral), the only adjustment we need is to change M to $(N'/N)\,M$ in α.

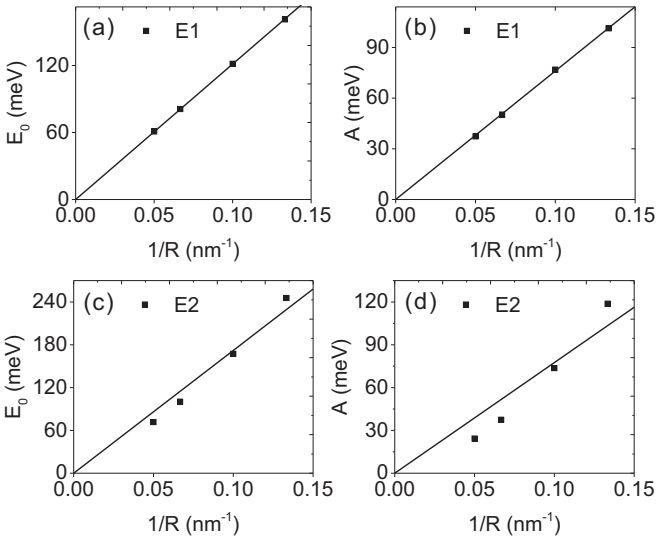

FIG. 7. The parameter E_0 and A for different radius R: (a) and (b) for $E1$ and (c) and (d) for $E2$. Symbols are the calculated values and lines are the linear fits. Here $N = 50$, $R = 7.5$, 10, 15, and 20 nm.

V. SUMMARY

In this work we have studied the effect of magnetic impurities on the local electronic structure on the surface of a TI by taking into account both the magnetic and potential scattering. For single impurity on TI, LDOS near the impurity shows distinct patterns of two resonance states with the positions depending on the ratio of U/M. However, when U/M is large, these two resonance states have very similar energy and become indistinguishable and only one single peak is observable. This could explain the current discrepancy between the STS and XMCD results. The presence of only one single peak makes it difficult to detect the effect of M. When the magnetic impurities form nanosized quantum corrals, we found that the effect of M can be significantly magnified and the spectra in the centers of the corrals strongly depend on both M and U. The relation between the strength of U, M, and the energy positions of the quantum well states are explored and a one-to-one correspondence is found. It provides a unique scheme to determine both U and M. The determination of both U and M may have great importance for future TI based device design.

ACKNOWLEDGMENTS

We thank Professor W. Y. Zhang at Nanjing University for helpful discussions. This work was supported by the National Key R&D Program of China (Grant No. 2017YFA0303202), the National Natural Science Foundation of China (Grants No. 51571109, No. 11374145, No. 51601087, and No. 11734006), and the Natural Science Foundation of Jiangsu Province (Grant No. BK20150565).

[1] M. Z. Hasan and C. L. Kane, Rev. Mod. Phys. **82**, 3045 (2010).
[2] X.-L. Qi and S.-C. Zhang, Rev. Mod. Phys. **83**, 1057 (2011).
[3] Y. Tanaka, T. Yokoyama, and N. Nagaosa, Phys. Rev. Lett. **103**, 107002 (2009).
[4] I. Garate and M. Franz, Phys. Rev. Lett. **104**, 146802 (2010).
[5] L. Fu and C. L. Kane, Phys. Rev. Lett. **100**, 096407 (2008).
[6] D.-X. Qu, Y. S. Hor, J. Xiong, R. J. Cava, and N. Ong, Science **329**, 821 (2010).
[7] Y. L. Chen, J. H. Chu, J. G. Analytis, Z. K. Liu, K. Igarashi, H. H. Kuo, X. L. Qi, S. K. Mo, R. G. Moore, D. H. Lu, M. Hashimoto, T. Sasagawa, S. C. Zhang, I. R. Fisher, Z. Hussain, and Z. X. Shen, Science **329**, 659 (2010).
[8] S.-Y. Xu, M. Neupane, C. Liu, D. Zhang, A. Richardella, L. Andrew Wray, N. Alidoust, M. Leandersson, T. Balasubramanian, J. Sánchez-Barriga, O. Rader, G. Landolt, B. Slomski, J. Hugo Dil, J. Osterwalder, T.-R. Chang, H.-T. Jeng, H. Lin, A. Bansil, N. Samarth, and M. Zahid Hasan, Nat. Phys. **8**, 616 (2012).
[9] L. A. Wray, S.-Y. Xu, Y. Xia, D. Hsieh, A. V. Fedorov, Y. S. Hor, R. J. Cava, A. Bansil, H. Lin, and M. Z. Hasan, Nat. Phys. **7**, 32 (2011).
[10] J. Honolka, A. A. Khajetoorians, V. Sessi, T. O. Wehling, S. Stepanow, J. L. Mi, B. B. Iversen, T. Schlenk, J. Wiebe, N. B. Brookes, A. I. Lichtenstein, P. Hofmann, K. Kern, and R. Wiesendanger, Phys. Rev. Lett. **108**, 256811 (2012).
[11] M. R. Scholz, J. Sánchez-Barriga, D. Marchenko, A. Varykhalov, A. Volykhov, L. V. Yashina, and O. Rader, Phys. Rev. Lett. **108**, 256810 (2012).
[12] T. Schlenk, M. Bianchi, M. Koleini, A. Eich, O. Pietzsch, T. O. Wehling, T. Frauenheim, A. Balatsky, J. L. Mi, B. B. Iversen, J. Wiebe, A. A. Khajetoorians, P. Hofmann, and R. Wiesendanger, Phys. Rev. Lett. **110**, 126804 (2013).
[13] P. Sessi, F. Reis, T. Bathon, K. A. Kokh, O. E. Tereshchenko, and M. Bode, Nat. Commun. **5**, 5349 (2014).
[14] M. Bianchi, R. C. Hatch, J. Mi, B. B. Iversen, and P. Hofmann, Phys. Rev. Lett. **107**, 086802 (2011).
[15] T. Valla, Z. H. Pan, D. Gardner, Y. S. Lee, and S. Chu, Phys. Rev. Lett. **108**, 117601 (2012).
[16] Q. Liu, C.-X. Liu, C. Xu, X.-L. Qi, and S.-C. Zhang, Phys. Rev. Lett. **102**, 156603 (2009).
[17] R. R. Biswas and A. V. Balatsky, Phys. Rev. B **81**, 233405 (2010).
[18] J.-J. Zhu, D.-X. Yao, S.-C. Zhang, and K. Chang, Phys. Rev. Lett. **106**, 097201 (2011).
[19] D. A. Abanin and D. A. Pesin, Phys. Rev. Lett. **106**, 136802 (2011).
[20] T. Eelbo, M. Waśniowska, M. Sikora, M. Dobrzański, A. Kozłowski, A. Pulkin, G. Autès, I. Miotkowski, O. V. Yazyev, and R. Wiesendanger, Phys. Rev. B **89**, 104424 (2014).
[21] T. Eelbo, M. Sikora, G. Bihlmayer, M. Dobrzański, A. Kozłowski, I. Miotkowski, and R. Wiesendanger, New J. Phys. **15**, 113026 (2013).
[22] M. Waśniowska, M. Sikora, M. Dobrzański, T. Eelbo, M. M. Soares, M. Rams, I. Miotkowski, R. Wiesendanger, R. Berndt, Z. Kąkol, and A. Kozłowski, Phys. Rev. B **92**, 115412 (2015).
[23] R.-Q. Wang, S.-H. Zheng, and M. Yang, New J. Phys. **18**, 093048 (2016).
[24] P. Thalmeier and A. Akbari, Phys. Rev. B **86**, 245426 (2012).
[25] A. M. Black-Schaffer, A. V. Balatsky, and J. Fransson, Phys. Rev. B **91**, 201411 (2015).
[26] C.-Y. Lin, A. H. Castro Neto, and B. A. Jones, Phys. Rev. Lett. **97**, 156102 (2006).
[27] G. A. Fiete and E. J. Heller, Rev. Mod. Phys. **75**, 933 (2003).
[28] M. F. Crommie, C. P. Lutz, and D. M. Eigler, Science **262**, 218 (1993).
[29] D. K. Morr and N. A. Stavropoulos, Phys. Rev. Lett. **92**, 107006 (2004).
[30] N. A. Stavropoulos and D. K. Morr, Phys. Rev. B **71**, 140501 (2005).
[31] N. A. Stavropoulos and D. K. Morr, Phys. Rev. B **73**, 140502 (2006).
[32] J. D. Walls and E. J. Heller, Nano Lett. **7**, 3377 (2007).
[33] H. Zhang, C.-X. Liu, X.-L. Qi, X. Dai, Z. Fang, and S.-C. Zhang, Nat. Phys. **5**, 438 (2009).
[34] Y. Xia, D. Qian, D. Hsieh, L. Wray, A. Pal, H. Lin, A. Bansil, D. Grauer, Y. S. Hor, R. J. Cava, and M. Z. Hasan, Nat. Phys. **5**, 398 (2009).
[35] T. Zhang, P. Cheng, X. Chen, J.-F. Jia, X. Ma, K. He, L. Wang, H. Zhang, X. Dai, Z. Fang, X. Xie, and Q.-K. Xue, Phys. Rev. Lett. **103**, 266803 (2009).
[36] D. K. Efimkin and V. Galitski, Phys. Rev. B **89**, 115431 (2014).
[37] J. Paaske and E. Gaidamauskas, Phys. Rev. Lett. **117**, 177201 (2016).
[38] J.-H. She, J. Fransson, A. R. Bishop, and A. V. Balatsky, Phys. Rev. Lett. **110**, 026802 (2013).
[39] Z.-G. Fu, P. Zhang, Z. Wang, and S.-S. Li, Phys. Rev. B **84**, 235438 (2011).
[40] Y. V. Skrypnyk and V. M. Loktev, Phys. Rev. B **73**, 241402 (2006).
[41] M. V. Berry and R. J. Mondragon, Proc. R. Soc. London Sect. A **412**, 53 (1987).
[42] A. Lobos and A. A. Aligia, Phys. Rev. B **68**, 035411 (2003).
[43] G. García-Calderón and L. Chaos-Cador, Phys. Rev. B **73**, 195405 (2006).
[44] P. Hewageegana and V. Apalkov, Phys. Rev. B **77**, 245426 (2008).
[45] G. J. Ferreira and D. Loss, Phys. Rev. Lett. **111**, 106802 (2013).
[46] R. Seshadri and D. Sen, Phys. Rev. B **89**, 235415 (2014).
[47] J. H. Bardarson, M. Titov, and P. W. Brouwer, Phys. Rev. Lett. **102**, 226803 (2009).
[48] L. A. Ponomarenko, F. Schedin, M. I. Katsnelson, R. Yang, E. W. Hill, K. S. Novoselov, and A. K. Geim, Science **320**, 356 (2008).
[49] C. Gutiérrez, L. Brown, C.-J. Kim, J. Park, and A. N. Pasupathy, Nat. Phys. **12**, 1069 (2016).